Available online at www.sciencedirect.com
ScienceDirect
Sensors and Actuators B 131 (2008) 254–264
SENSORS AND ACTUATORS B CHEMICAL
www.elsevier.com/locate/snb

A CMOS-based integrated-system architecture for a static cantilever array

M. Zimmermann [a], T. Volden [a], K.-U. Kirstein [a], S. Hafizovic [a], J. Lichtenberg [a], Oliver Brand [b], A. Hierlemann [a,*]

[a] *Physical Electronics Laboratory, ETH Zurich, ETH Hoenggerberg, HPT H4.2, Wolfgang-Pauli-Strasse 16, CH-8093 Zurich, Switzerland*
[b] *School of Electrical and Computer Engineering, Georgia Institute of Technology, Atlanta, GA 30332-0250, USA*

Received 6 July 2007; received in revised form 17 October 2007; accepted 12 November 2007
Available online 22 November 2007

Abstract

A monolithic, integrated sensor system architecture is presented that features microcantilevers operated in the deflection mode as transducer elements for detecting (bio)chemical compounds. The cantilevers have been coated with polymer layers to detect volatile organic compounds, such as ethanol. The analyte-sorption-induced surface-stress changes of the cantilevers have been detected by piezoresistive Wheatstone bridge configurations embedded in the cantilevers. The integrated readout circuitry includes a chopper-stabilized amplifier, which performs a low-noise, low-offset amplification of the μV-range sensor signal. Additional low-pass filtering and a programmable offset compensation stage on the chip provide a good signal-to-noise ratio. A sigma–delta analog-to-digital converter (ΣΔ-ADC) delivers the measured data to the outside world via a digital serial interface. The monolithic integration reduces the sensitivity to external interference and enables autonomous device operation. The focus of the paper is on the system design and integration, which can also be applied to other types of cantilevers or cantilevers featuring different geometries.

Keywords: CMOS; Cantilever; Static cantilever; Deformation; Stress; Piezoresistor; Wheatstone bridge

1. Introduction

Cantilevers have been widely used in atomic-force microscopy (AFM) [1–3] and as chemical and biosensors [4–27]. Complementary-metal-oxide-semiconductor (CMOS)-based cantilevers consist of a layered structure of, e.g., the dielectric layers of a standard CMOS process, silicon, metallizations, and, eventually, additional piezoelectric or piezoresistive materials [13,16,22,23,28]. The cantilever base is firmly attached to the silicon support. The freestanding cantilever end is then coated with a sensitive material.

Generally, there are two different ways to operate a cantilever as a chemical sensor, (a) the *static mode*, in which the cantilever deflection upon stress changes in the sensitive layer is measured [4,11,12], and (b) the *dynamic mode*, in which the cantilever is excited in its fundamental mechanical resonance, and in which the resonance frequency change upon mass loading in the sensitive layer is recorded [5,6,8,13,16,22]. These two modes impose completely different constraints on the cantilever design: the static mode requires long and deformable cantilevers, whereas the dynamic mode requires short and stiff cantilevers to achieve high operation frequencies [13,16,22,23,28]. In contrast to previous publications on dynamic cantilever arrays [13,16,22,23,28–30], we want to present here a fully integrated CMOS-based static cantilever array.

Cantilever beams have been shown to deflect, when their surface properties are changed by binding events [23]. This is interpreted as a change in the surface-stress of the cantilever, related to the new composition of the surface layer. Sterical hindrance of large, densely packed molecules is one of the mechanisms responsible for the stress change. A surface-stress change induces a bending of the cantilever and a stress in the cantilever material. The cantilever deformations can be detected using optical methods by means of laser light reflection on the cantilever [4,11,12,17–21] or electrically by embedding piezoresistors or stress-sensitive transistors in the cantilever base [5,8,13,15,16,22], or by measuring deflection-induced capacitance changes [6,7,29,30]. Optical read-out of the cantilever deflection is, due to its high sensitivity and the availability of existing AFM equipment, very popular. However, the

* Corresponding author.
E-mail address: hierlema@phys.ethz.ch (A. Hierlemann).

0925-4005/$ – see front matter © 2007 Elsevier B.V. All rights reserved.
doi:10.1016/j.snb.2007.11.016

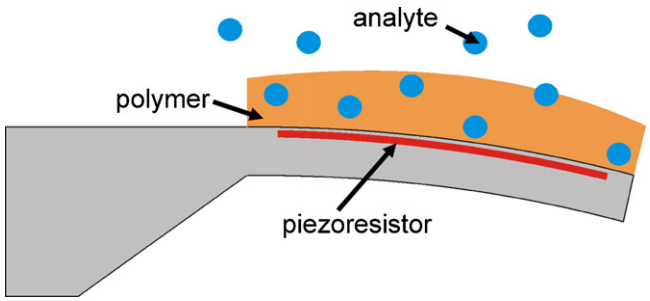

Fig. 1. Change of surface-stress on a microcantilever due to absorption of an analyte.

read-out can be affected by both, the opacity and the refractive index of the liquid samples. The laser beam can also heat the cantilever and cause parasitic deflection [31]. Moreover, the optical read-out is technically difficult to scale to large cantilever arrays, which would allow the simultaneous detection of multiple analytes [4,17]. Piezoresistive read-out, on the other hand, is well suited for cantilever arrays and compact systems, where the sensor is integrated with electronic circuitry, as well as for microfluidic total analysis systems (μTAS) [13,15,16].

A schematic of the integrated sensor device for detecting gas phase analytes, such as water vapor or volatile organic compounds is shown in Fig. 1. A polymer or receptor layer is deposited on one side of the cantilever [8]. The absorption of the analyte in the polymer/receptor layer increases the polymer volume and acts mechanically on the cantilever in the same way as a change in the surface-stress. The resulting change in the resistivity of the piezoresistor embedded in the cantilever will then be amplified and filtered on chip. By using adequate surface functionalization techniques, the sensor system can be used for a large spectrum of chemical and biochemical applications [32].

In the next sections the focus will be on the system architecture and integration: the different components, i.e., the cantilever transducer and the circuitry units of the CMOS integrated cantilever microsystem will be described. Before designing the system some major issues had to be addressed. There is a long time constant for most chemical and biochemical processes so that the system had to be designed with a low bandwidth (i.e., 1 sample/s). The sensor signals are on the order of microvolts, so low-noise, high-gain amplification was required. Fabrication and functionalization introduce sensor offsets in the millivolt range, which has to be handled by the circuitry to avoid saturation of the signal chain.

Finally, mechanical, electrical and chemical sensor characterization results of the system will be shown.

2. Cantilever transducer

Due to its well-defined mechanical properties, crystalline silicon has been chosen as the main cantilever material, which also allows for the implantation of piezoresistors during the CMOS process. The use of an electrochemical etch-stop in the postprocessing provides an initial silicon thickness of 3.5 μm with the possibility of additional RIE (reactive-ion etching) thinning.

The cantilever design was optimized so that the local cantilever bending to be directly transduced through the piezoresistors, the design was not optimized for end-point deflection. In fact, a large sensitivity to the end-point deflection would be detrimental, since flows in the media surrounding the cantilever would also be picked up. The length and width of the cantilever are 300 μm, which is almost 100 times the thickness of the silicon layer. Since the surface-stress change to be detected is in principle isotropic and uniform over the functionalized surface, the lateral size and shape of the cantilever do not directly influence the sensitivity of the sensor. This is in contrast to similar sensors based on optical read-out, which measures the tip deflection of the cantilever. The tip deflection is quadratic to the length of the cantilever for a small, uniform bending, and, therefore, long cantilevers are usually preferred for optical read-out schemes. Using integrated sensors, the bending moment caused by the surface-stress is directly and locally affecting the piezoresistors. The distribution of the active area also means, that the width does not have the same significance as in the detection of concentrated forces (as seen in AFM applications), since the surface-stress change is constant over the active surface area and independent of the width. However, for the surface-stress to effectively be transferred into the transducer sensitive elements, the cantilever length and width should be large in comparison to the cantilever thickness: stress release at the edges reduces the stress field in the border region, the extension of which increases with the relative cantilever thickness.

The piezoresistors are protected from the environment by layers of silicon oxide and silicon nitride. However, the protection layers separate the functionalization layer from the sensing piezoresistive layer and decrease the sensitivity of the sensor system. They should therefore be as thin as possible while still providing sufficient protection. The CMOS process provides several silicon dioxide layers that can be left on top of the cantilever, as well as the final silicon nitride passivation, especially engineered for protection of the chip circuitry. Although the silicon nitride layer would give sufficient protection, the process flow does not allow for the removal of all the oxides without degrading the piezoresistive layer. Therefore, a sandwich of thermally grown field oxide and deposited (CVD) oxides is left on the cantilever after the CMOS process (see Fig. 2). The thickness of the silicon dioxide layers is 1.6 μm on top of a diffusion layer and 2.1 μm elsewhere. The silicon nitride layer is 1.0 μm thick

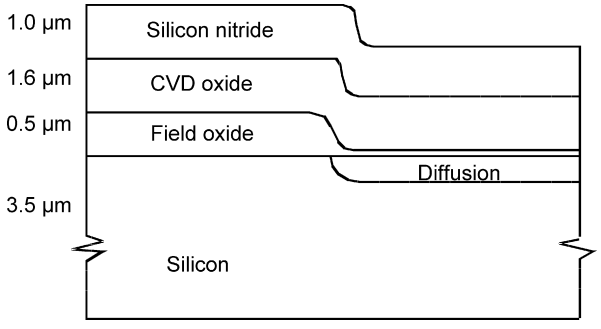

Fig. 2. Cross-section of a cantilever (not to scale). The right part contains a diffused resistor, with a reduced thickness of the oxide layers.

Another issue concerns the design of the piezoresistors embedded in the cantilever. As a stress in the piezoresistive layer causes a relative change of resistivity, the absolute resistance does not directly influence the sensitivity. As is evident from simulations [33], the stress field has only distinct concentration regions close to the clamped edge. Due to the uncertainty of the edge location after the micromachining, these regions are not ideal for placing the resistors. Other than very close to the free and clamped edges, there are no large variations in the stress field that would indicate a preferred resistor location.

However, the resistor design greatly affects the internal noise characteristics. The thermal noise power is proportional to the resistance and to the signal bandwidth, suggesting the use of a small resistance. However, since the bandwidth of the target signals is narrow (from 1 mHz to 1 Hz), the thermal noise is not dominant. The flicker noise, on the other hand, becomes important for low-frequency measurements, because the chopper amplifier removes only the $1/f$ noise of the amplifier itself but not that of the input signal, since the resistors are not located between the input and output modulators of the chopper amplifier. A chopper amplifier is used to keep the total noise in the amplified signal low. The spectral density of the flicker noise is inversely proportional to the frequency and to the total number of charge carriers in the resistor. The volume occupied by the resistor should therefore be as large as possible in order to maximize the number of charge carriers.

A large enough resistance is also required to avoid self-heating of the sensor and to match the input stage of the subsequent amplification circuitry. The sensors were, therefore, designed with 10 kΩ resistors, yielding a power dissipation of 2.5 mW per resistor for a bridge voltage supply of 5 V. With the ratio between width and length given by the targeted resistance R and the sheet resistance R_S, the resistor is laid out in a meander structure to cover as much as possible of the available area (Fig. 3). This minimizes the flicker noise and averages the sensor output over the largest part of the cantilever. The p+ diffusion used for the resistors has a sheet resistance of 40 Ω. With 300 μm × 300 μm cantilever plates and two resistors on each cantilever, a total resistor length of 2130 μm was obtained using a width of 8.5 μm. Simulations revealed how the clamping of the cantilever plate alters the stress distribution in the sensing layer, resulting in a larger stress change parallel to the cantilever axis [33]. The resistors are therefore mainly aligned along the cantilever axis.

The sensor chips feature an array of cantilever sensors together with signal conditioning and interface circuitry. Four cantilevers, equally spaced at a pitch of 500 μm, are located along one side of the chip in order to simplify the packaging (Fig. 4). Different measurement configurations have been explored: all cantilevers can be individually functionalized to detect different analytes. Alternatively, one or more cantilevers can act as a reference sensor by being functionalized to not bind analytes. This is a way to discriminate non-specific binding and other parasitic signals. Different configurations of the piezoresistive Wheatstone bridges have been fabricated and evaluated [33].

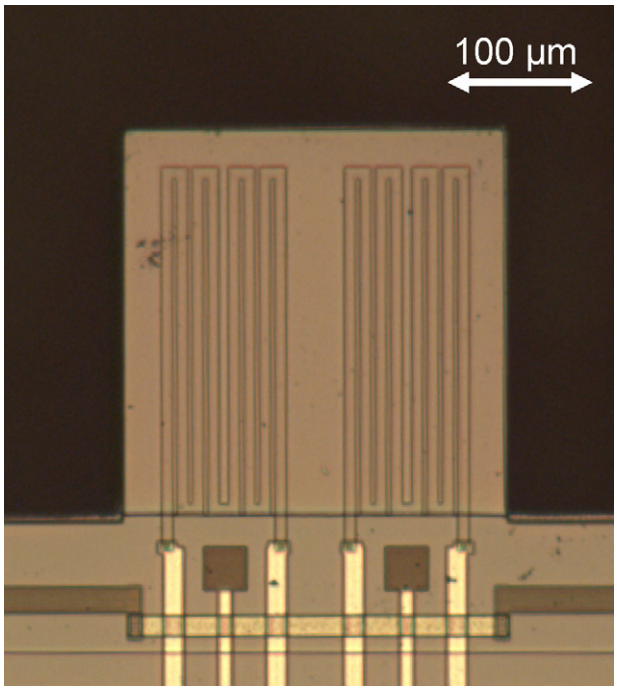

Fig. 3. Micrograph of one cantilever. The cantilevers have dimensions of 300 μm × 300 μm × 5 μm. A p+ diffusion of the CMOS process is used to integrate two piezoresistors of 10 kΩ on each cantilever. These p+ diffusion piezoresistors act as surface-stress sensors.

Fig. 4 shows the micrograph of the cantilever array. The sensing cantilevers (2nd and 4th cantilever in the array from the left) have an additional gold layer on top, while the reference cantilevers (1st and 3rd) have only silicon nitride as protective layer on the surface. The gold layer will allow to apply, e.g., thiol-based functionalization chemistry. Sensing and reference cantilevers are paired (a gold-coated sensing cantilever and an uncoated reference cantilever) to achieve a dual-cantilever symmetric Wheatstone bridge configuration: two resistors are located on cantilever 1, two on cantilever 2. Placed on otherwise identical cantilevers, the resistors are well matched, resulting in a minimal offset voltage. Common-mode signals affecting both cantilevers are directly cancelled out by the bridge design. The Wheatstone bridge output features a deflection sensitivity of 0.7 μV/nm per Volt bias voltage, and the offset of the Wheatstone bridge is 25 ± 5 mV at 5 V bias voltage.

3. System architecture and circuitry components

The electronic circuitry is designed for high-gain amplification of the sensor output signal, while maintaining low-noise characteristics and providing the possibility of sensor offset compensation. Fig. 5 shows the block diagram of the sensor system. The input multiplexer connects one sensor of the sensor array at a time to the analog front-end. The weak output signal of the sensor is first amplified by a low-noise chopper amplifier (see Fig. 6). After low-pass filtering and offset compensation, the signal is further amplified in two gain stages, the gains of which are tunable. Before the signal is converted to the digital domain by a 2nd-order single-bit ΣΔ-modulator, it passes an anti-aliasing

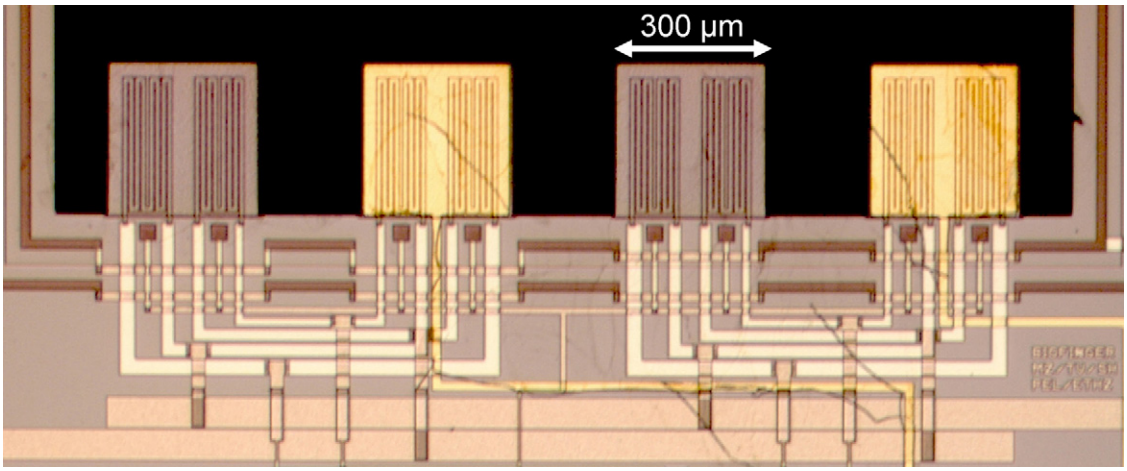

Fig. 4. Sensor array with four microcantilevers. Sensing and reference cantilever are paired (gold-coated sensing cantilever, and uncoated reference cantilever) to achieve a dual-cantilever symmetric Wheatstone bridge configuration: two resistors are located on cantilever C_1, two on C_2.

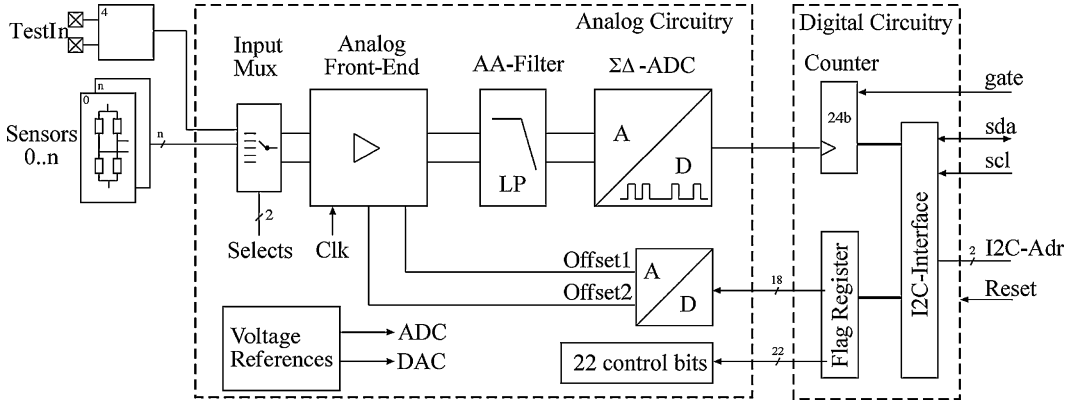

Fig. 5. Block diagram of the sensor system: sensor array, multiplexer, amplifiers and filters are integrated on a single chip along with a digital block. The analog signal chain is fully differential.

filter. The compensation voltages for the offset compensation are generated on the chip with two digital-to-analog converters (8 bit and 10 bit).

The digital back-end consists of a simple decimation filter and an addressable serial bus interface. The digital interface and the on-chip voltage references for the analog-to-digital converter (ADC) and the digital-to-analog converters (DACs) help to reduce the number of bond pads, which leads to reduced packaging costs and increased reliability.

The fully differential architecture of the analog front-end increases the dynamic range and improves the signal-to-noise ratio of the whole system. For testing purposes, the system has several test inputs and outputs, which provide flexibility for in-system testing of almost every single building block. In the following, key components will be described in more detail.

3.1. Chopper amplifier

The chopper amplifier consists of a wide-band one-pole amplifier between the input and output modulator (Fig. 6). The wide-band amplifier minimizes the introduced phase shift and makes the DC gain of the chopper amplifier less sensitive to this phase shift [34]. The input and output mixers consist of four cross-coupled switches and are controlled by a square-wave

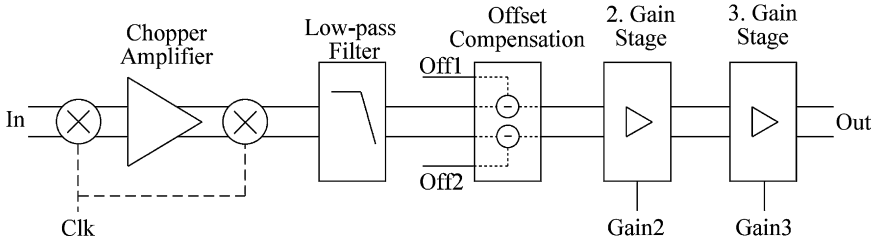

Fig. 6. Block diagram of the analog front-end in Fig. 5.

clock signal with a duty cycle of 50%. Since the input signals are very small, NMOS switches in the input mixer can be used, while CMOS switches in the output modulator improve the dynamic range of the chopper. Due to the fully differential configuration of the system, charge injection in the mixers causes changes in the common-mode signal, which are greatly attenuated by the common-mode rejection characteristics of the subsequent amplifier.

The wide-band amplifier is based on a degenerated differential pair with transconductance enhancement (Fig. 7). Its gain is defined by the ratio of R_{load} to R_{conv} [35]. By closing the HG-switches (high-gain) in the enhancement loop, R_{conv} is minimal, and, thus, the gain is maximal. LG-switches set the minimum gain (low gain). The added common-mode feedback (CMFB) circuit, consisting of transistors T1–T6, controls the common-mode voltage of the amplifier output. This add-on to the amplifier presented in [35] renders the output common-mode voltage independent of the resistor process spread, which is important especially with respect to the needed high-gain and large dynamic range. The output common-mode, CM_{out} in Fig. 7, is fed back to the input of a simple differential input stage, where it is compared to the desired common-mode voltage, V_{CM}. The output of this single-stage amplifier controls the gate voltages of T5 and T6. A change of the transistor output resistance directly influences the output common-mode voltage.

The upper current sources of the operational amplifier in Fig. 7 are implemented as self-biased high-swing cascade current sources [36], while the lower current sources are built up as regulated cascade circuits [37]. The usage of these special types of current sources maximizes the dynamic range of the operational amplifier. The biasing part of the self-biased, high-swing cascade current source is also shown in Fig. 7 (T7, T8, and R_b). This special type of current mirror needs only one reference current and thus helps to minimize the power dissipation. If the voltage drop over R_b is equal to the saturation voltage of T7, assumed that T7 and T8 have both the same saturation voltage, all the transistors in the current mirror work in the saturation mode.

To minimize the chip area of the low-pass filter on the one hand and to limit the necessary wide-band amplifier bandwidth on the other hand, a chopping frequency of $f_{chop} = 10$ kHz has been chosen. This frequency is high enough with respect to the $1/f$ corner frequency of the amplifier of about 1 kHz (value from circuitry simulations) to result in an upper corner frequency of the chopper amplifier, which is cut off by the following low-pass filter [34,38]. The gain of the chopper amplifier can be set to 20 or 40 and, owing to the large dynamic range of the operational amplifier, a sensor offset of up to 100 mV can be handled.

3.2. Low-pass filter and offset compensation

Two 2nd-order Sallen-Key low-pass filters in a pseudo-differential configuration with $f_{-3dB} = 500$ Hz reconstruct the original signal after the chopper demodulator and cut off the low-frequency noise and offset of the wide-band amplifier, which are moved to the odd harmonics of the chopping frequency. The finite bandwidth of the chopper amplifier and the non-delayed demodulation cause high frequency signal spikes, which the low-pass filter has to attenuate in order to prevent the following gain stages from saturation. In the offset compensation stage, a difference amplifier subtracts a differential voltage from the signal path. As shown in Fig. 5 this compensation voltage is derived from two digital-to-analog converters, which are programmable via the digital interface.

3.3. Gain stages

The signal is further amplified in two additional gain stages. The structure of these two amplifiers is the same as that of the chopper amplifier. The gain of the 2nd amplification stage can be set to 4 or 16, while the 3rd gain can be 4 or 8. Together with the chopper amplifier a minimum gain of 320 and a maximum

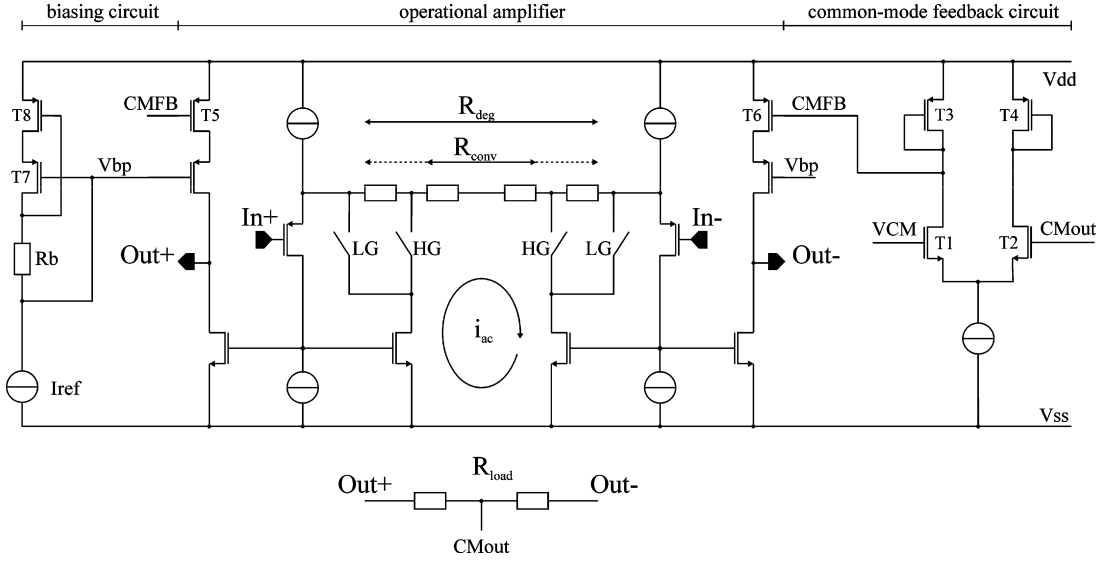

Fig. 7. Schematic of the chopper operation amplifier.

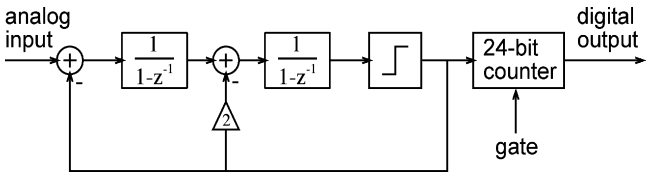

Fig. 8. Block diagram of the Sigma–delta analog-to-digital converter.

gain of 5120 can be achieved. An additional gain of 4 can be set in the Sigma–delta ADC by only changing the clocking scheme.

3.4. On-chip voltage references

The voltage references for the ADC and the DACs (offset cancellation) are derived from an on-chip band-gap voltage reference. The reference for the ADC can be tuned in order to adjust its dynamic range to the input signal. The use of on-chip voltage references minimizes the number of pads and improves the signal-to-noise characteristics of the system.

3.5. Sigma–delta-AD converter

A single-bit, second-order Sigma–delta ($\Sigma\Delta$) modulator performs the conversion of the amplified and filtered sensor signal to the digital domain. Fig. 8 shows a block diagram of the converter architecture. The two loop filters are discrete time integrators in fully differential switched-capacitor-circuit technology. The output of the $\Sigma\Delta$ modulator is connected to a 24 bit digital counter for decimation of the digital signal. As the target applications feature signals of low bandwidth (usually below 1 Hz), a decimation filter of higher order is not needed. The sampling frequency of the modulator is 100 kHz, and the characterization of the ADC has been performed with a gate time of 1 s for the counter, leading to an oversampling ratio (OSR) of 100,000.

3.6. Circuitry back-end

The bidirectional, addressable, industrial standard I^2C bus interface [39] is complemented by the 24 bit decimation counter and by a flag register to store a set of 40 control bits. These bits control the input multiplexer, tune the different gain stages, set the DACs for the offset compensation and operate the system in different test modes. An external gate signal triggers the decimation counter. Every time the counter is gated, its content is copied into an extra register, where it can be read-out by the interface, while the counter continues counting. This way, a conversion rate that depends on the gate signal is achieved, and the oversampling ratio of the single-bit $\Sigma\Delta$ modulator can be adapted to the desired final resolution.

4. Chip fabrication and packaging

A micrograph of the single-chip sensor system is shown in Fig. 9. The chip size is 5.2 mm × 2.7 mm including the silicon lugs on each side of the cantilever array. The system consumes approximately 50 mW power at a supply voltage of 5 V. The cantilever-based sensor chip has been fabricated in a standard 0.8 μm double-poly, double-metal CMOS process with post-CMOS micromachining. After completion of the CMOS process, a back-side anisotropic silicon etch is performed using potassium hydroxide (KOH) and an electro-chemical etch-stop technique. The pn-junction for the etch-stop is defined by the *n*-well diffusion of the CMOS technology, so that the depth of the *n*-well diffusion determines the thickness of the monocrystalline

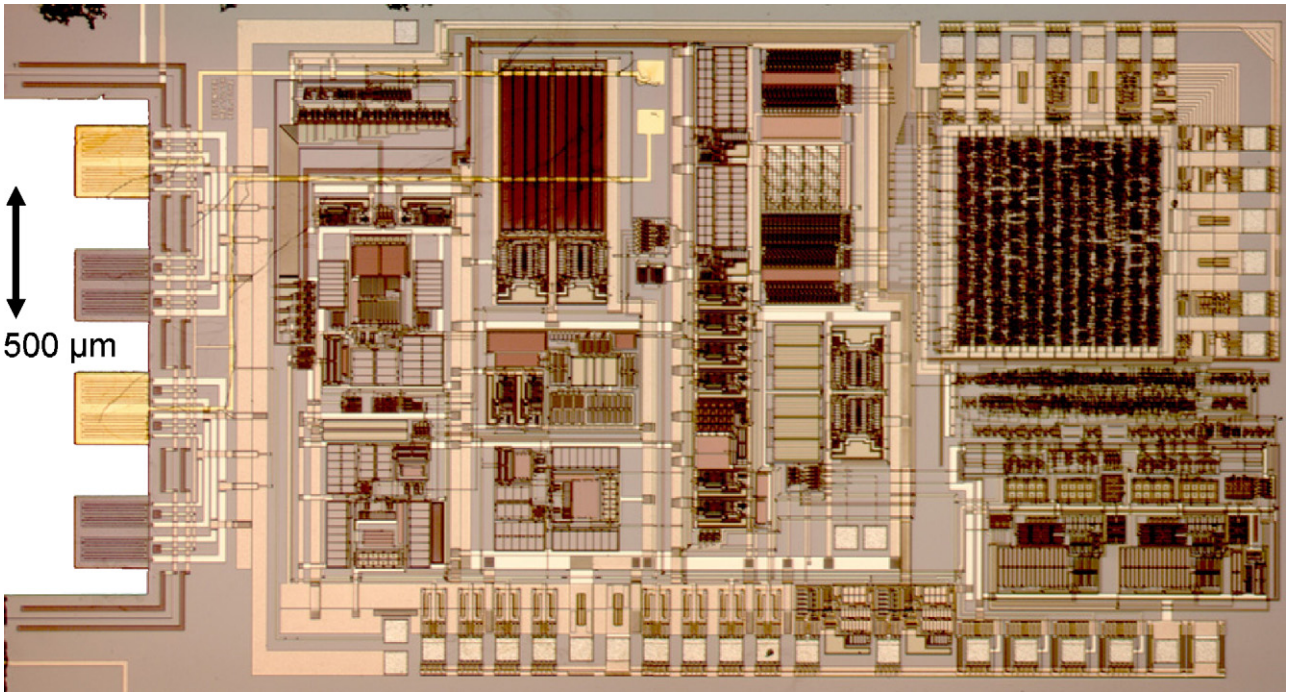

Fig. 9. Micrograph of the single-chip sensor system.

silicon layer of the cantilevers [40]. For testing purposes the chip has been manually packaged into a ceramic DIL-package.

5. Results

5.1. Mechanical characterization

A common way of characterizing AFM cantilevers with integrated deflection sensors is to deflect the cantilever by a force on its tip, usually in order to obtain a known deflection, z, and to then measure the corresponding sensor output, V. The stiffness, k, can be determined from resonance frequency measurements, since the resonance frequency is a function of the stiffness and the mass only. The mass, or equivalent mass in the case of non-rectangular cantilevers, is calculated from the cantilever dimensions and material density. The applied force is then found with $F = kz$, and the sensitivity, S, in terms of sensor output per applied force can be calculated:

$$S = \frac{V}{F} = \frac{V}{kz} \quad (1)$$

This method can also be applied to the surface-stress sensors. However, it is important to keep in mind that the force distribution upon applying this mechanical method is different from the one caused by a surface-stress change, so that the resulting sensitivity, S, does not directly translate into a measure of the surface-stress sensing capabilities. Deflection measurements were performed with the help of a piezoelectric actuator (piezotube). The cantilever chips were glued to small printed circuit boards, which were mounted on a custom-made metal holder to fit into the scanning stage of a commercial AFM system (Multimode MMAFM-2, Veeco Instruments Inc.). A small wedge made from anisotropically etched silicon was placed on top of the piezotube, where normally the sample to be scanned is located. The cantilever was then positioned to touch the wedge with its outer edge (Fig. 10). By actuating the piezotube in z-direction, an almost vertical force could then be exerted on the contact point of the cantilever edge. The force constant of the cantilever, k, was found to be 28 ± 3 N/m (simulation: 26 N/m). The Wheatstone bridge output featured linear characteristics (values between 0 and 4.5 V) over a deflection range of 1200 nm (Fig. 10), which results in a deflection sensitivity of 0.74 μV/nm per Volt power supply. The offset of the Wheatstone bridge was $25\,\text{mV} \pm 5\,\text{mV}$ at 5 V power supply (average of approximately 15 sampled amplifiers). Noise measurements of a cantilever in a non-contact situation (no contact with the wedge) indicated a noise-level of 3 μV, with a resulting detection limit of 2 nm (three times RMS noise) at 5 V bias.

5.2. Electrical and circuitry characterization

The sensors and electronic circuitry are tightly integrated on the chip and cannot be taken apart. There are, however, ways to decouple the sensors in order to measure the circuitry part on its own. The input multiplexers provide an additional channel for an external, differential signal to be fed to the input amplifiers. The response of the circuitry to an injected test signal can, therefore, be characterized in terms of gain and frequency response. Stand-alone sensors have also been tested, with an alternative instrumentation path and external amplification.

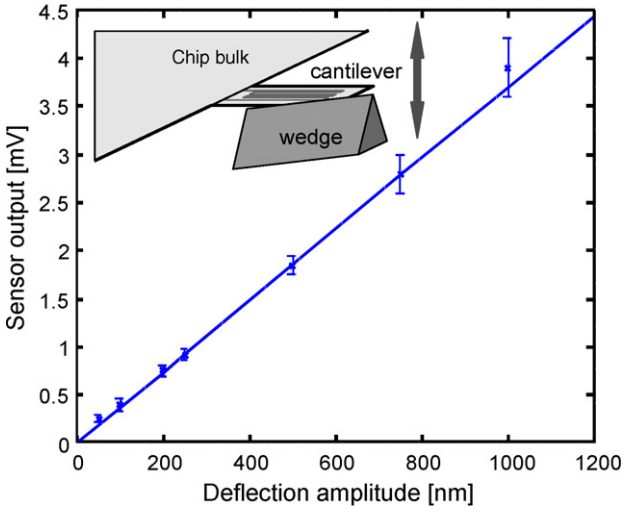

Fig. 10. Sensor output (5 V bridge bias) as a function of the deflection amplitude for a test sensor without integrated electronics. The linear approximation (solid line) has a slope of 3.7 μV/nm, equivalent to a deflection sensitivity of 0.74 μV/(nm V). The inset shows a schematic of the mechanical deflection measurement. The cantilever is bent by a punctual force on its free end applied through the wedge, which is moved vertically by a piezotube. The silicon wedge has been fabricated using anisotropic silicon etching.

The offset voltage of the Wheatstone bridges has been measured directly on test structures without on-chip circuitry. For dual-cantilever configurations the offset was 1–3 mV at 5 V bias, which is within the specifications of a "low-offset" circuitry design (5 mV). The most important characteristics of the sensor readout circuitry are summarized in Table 1.

To test the performance of the whole system and to assess the system accuracy an additional input to the input multiplexer has been used. The input voltage has been increased in defined steps, while the digital output of the system has been read-out via the I^2C interface. The absolute accuracy of the sensor system is shown in Fig. 11 and includes offset, gain, and integral linearity errors and also the quantization error of the ADC. The maximum total error is 8 mV. The characterization of the ADC evidences a resolution of 13 bit for the ADC only. This leads to an overall accuracy of better than 8 bit.

To characterize the combination of ΣΔ-ADC and the simple counter decimation filter, an extra voltage input to the ADC has been used. Fig. 12 shows the 8192-point fast-Fourier transform plot of the decimation filter output read through the I^2C bus.

Table 1
Characteristics of the readout circuitry

Tunable DC gains (dB)	50, 56, 62, 68, 74
−3 dB bandwidth	520 Hz
Input-referred front-end noise in the bandwidth of 10 mHz to 10 Hz	1.01 μV
S/N ratio of ADC @ 1 S/s	78 dB
System accuracy	8 bit
Chopping frequency	10 kHz
Sampling frequency	100 kHz

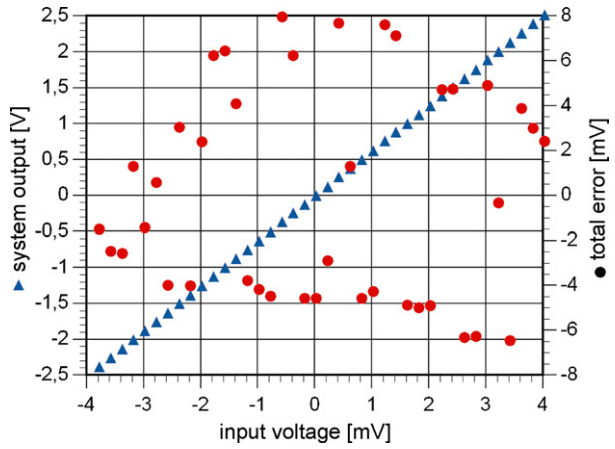

Fig. 11. Linearity plot of the sensor system. A gain of 640 and a full-scale range of 2.5 V for the ADC have been used.

The input signal amplitude has been set to 83% of the full scale. The modulator was operated at a frequency of 100 kHz, which yielded a conversion rate of 1 S/s at an oversampling ratio of 100,000. As can be derived from the spectrum in Fig. 12, a signal-to-noise ratio of better than 78 dB has been achieved. This corresponds to a resolution of 13 bits. The measured resolution is limited by the spurious levels and the harmonic distortion of the used external signal generator, which is, according to the generator manual, less than −62 dB for the used test signal.

The measured resolution is mainly limited by the performance of the external signal generator.

5.3. Sensor characterization: humidity and volatile organics

In order to reproducibly generate a distributed surface-stress, polymer coatings have been studied as a test system. The humidity-induced swelling of polymers has been investigated previously for the development of humidity sensors [41–44]. Silicon membranes were coated with polyimide, and the stress in the membranes was correlated to changes of the ambient humidity. The same effect can be observed with cantilever sensors [45].

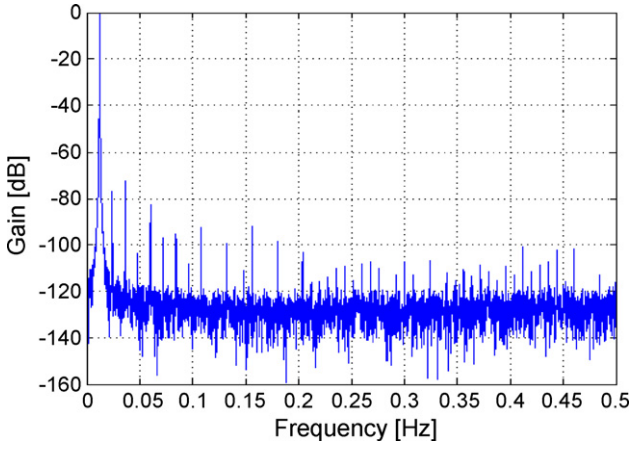

Fig. 12. Measured spectrum of the ΣΔ-ADC upon a sine-wave input signal at 12.207 mHz. The resulting SNR was 78 dB.

The expansion of the polymer can be expected to create the equivalent to a surface-stress change on the cantilever (Fig. 1). A known expansion can be used to quantify the surface-stress sensitivity of the sensor.

One of the measuring cantilevers was drop-coated with a positive photoresist (Shipley S1818: mixture of 70% propyleneglycolmethyletheracetate, 20% Novolac resin and 10% diazonaphtoquinone) as sensitive layer, while the respective reference cantilever was kept uncoated. The layer thickness was approximately 10 μm. The photoresist was cured in an oven at 100 °C for 30 min. The humidity cycling was performed in a climate chamber (SB-305, Weiss Umwelttechnik, Reiskirchen, Germany). A Labview (National Instruments) program on an external computer controlled the humidity and temperature settings of the climate chamber. The temperature was kept constant and was verified by the internal temperature sensor of the chamber (precision ± 0.1 K). The sensor output was measured for three cycles between 30 and 80% RH at a humidity change rate of 0.67%/min. The sensor output has been low-pass filtered (moving average of 100 samples at a sample rate of 1 Hz) in order to better distinguish the respective cycles. A linear humidity response was found (0.2–1.2 mV for 30–80% RH), but also hysteresis effects, i.e., an offset of approximately 0.2 mV between the humidity-increase cycle and the humidity-decrease cycle occurred. The sensitivity in either the increase or decrease cycle was determined to be 18 μV/% RH, with a resolution of 3% RH (three times RMS noise). With the same climate chamber, the sensors were also submitted to temperature cycling between 25 and 30 °C, while the relative humidity was kept constant at 50% RH, which is very similar to a real-world application scenario. The determined sensitivity to temperature was 110 μV/K. This is a rather large value, and it has to be noted that a new water partitioning equilibrium is established upon a temperature change, since the relative humidity has been kept constant throughout the temperature range. So the sensor monitors changes in the water molecule concentration in the polymer in addition to the effects of the thermal expansion of the polymer.

To further demonstrate the sensor functionality, the detection of volatile compounds was performed using a version of the chip featuring an analog read-out. The system was exposed to ethanol vapor at concentrations from 1200 ppm to 3600 ppm in a computer-controlled manifold. The CMOS chips were loaded into the measurement chamber of a gas manifold featuring a cross-over flow architecture. This cross-over flow architecture has two input gas lines, one supplying pure carrier gas and the other supplying carrier gas with defined doses of the volatile analyte, and two output gas lines, one leading to the measurement chamber, the other leading directly to the exhaust. This architecture offers the advantage that both input flows and both output flows are continuously flowing and the build-up time of a certain analyte concentration does not influence the dynamic sensor responses. The overall gas volume between the valve and the sensors was approximately 1.6 ml, which entails a time span of approximately 0.5 s after switching the valve until the gas reaches the sensors at the applied flow rate of 200 ml/min. The analyte vapors were generated from specifically developed temperature-controlled vaporizers using synthetic air as a carrier

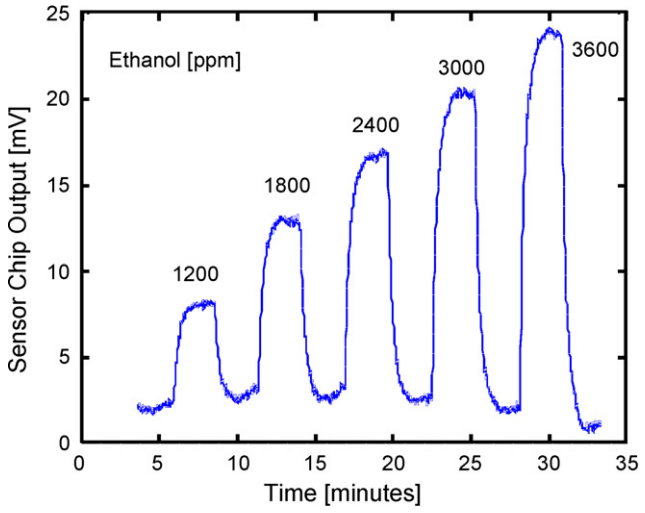

Fig. 13. Sensor response of a cantilever coated with photoresist to ethanol in the gas phase at concentrations from 1200 ppm to 3600 ppm. The chip gain was 320 and the bridge bias was 5 V.

gas, and then diluted as desired using computer-driven mass-flow controllers. The internal volume of these vaporizers, which distribute the liquid over a large-area packed-bed type support to maximize surface-to-volume ratio, was dramatically smaller than that of typical gas-washing bottles ("bubblers") [46]. The vapor-phase concentrations at the respective temperatures were calculated following the Antoine equation [47]. The sensor measurements were performed in a thermo-regulated chamber at a temperature of 30 °C. Both gas streams (pure carrier gas and carrier gas with analyte) were thermostabilized at the measurement chamber temperature before entering the chamber. Typical experiments consisted of alternating exposures to pure synthetic air and analyte-loaded synthetic air. Exposure times of 5–10 min to analyte-loaded gas (to reach thermodynamic equilibrium) were followed by 5–10 min purging the chamber with pure synthetic air. For details of the setup, see Ref. [48].

A bridge bias of 5 V and an amplification gain of 320 were used. The sensor response to ethanol gas is shown in Fig. 13. The ethanol concentration was ramped from 1200 ppm to 3600 ppm in steps of 600 ppm. A slight baseline drift has been observed. The chip output sensitivity is 6 μV/ppm, which corresponds to a detection limit of 250 ppm ethanol (three times the background noise level). This detection limit is by a factor of approximately 5 higher than that of, e.g., a resonating cantilever featuring 3 μm-thick poly(etherurethane), PEUT, or ethylcellulose, EC, coatings [16,49]. The equivalent sensor sensitivity, which is the voltage per applied voltage on the Wheatstone bridge per concentration and includes the gauge factor of the sensors, was 5 nV/(ppm V). The gauge factor includes the biasing voltage of the bridge and the total gain of the on-chip amplifier. As can be seen in Fig. 13, the response to ethanol has a time constant of 25 s, which is quite fast given the thickness of the polymer layer. Toluene was tested as a second analyte and showed considerably slower sorption characteristics (larger molecule). The chip output sensitivity was 3 μV/ppm, which is probably a consequence of the nonpolar character of toluene and the related lower sorption constant in a polar matrix.

6. Conclusion and outlook

A monolithic, integrated sensor system architecture has been presented that features microcantilevers as transducer elements for the detection of (bio)chemical compounds. The analyte absorption or binding produces changes in the surface-stress of the cantilevers, which is detected by an integrated piezoresistive Wheatstone bridge. The integrated readout circuitry includes a chopper-stabilized amplifier, which performs a low-noise, low-offset amplification of the μV-range sensor signal. Additional low-pass filtering and a programmable offset compensation stage allow for a high signal-to-noise ratio. A Sigma–delta analog-to-digital converter (ΣΔ-ADC) delivers the measured data to the outside world via a digital serial interface. The integrated-system architecture can be scaled to higher numbers of cantilevers and will be, in a next step, packaged and prepared for liquid-phase operation.

As already stated above, the analyte sensitivity of this system is by a factor of approximately 5 lower in comparison to a resonant-cantilever system [16,49], and, particularly, for analytes like humidity or ethanol, capacitive microsensors perform pronouncedly better [48,50]. So it is a valid question, whether it is worth the pain to further develop CMOS-integrated static cantilevers for gas sensor applications. On the circuitry side, a lot of efforts have been made as detailed in this paper. Certainly, the cantilever geometry can be optimized to increase the sensitivity, but we nevertheless anticipate future applications of such cantilevers more in the liquid regime than in the gas phase. Many issues have to be addressed for liquid-phase applications, such as flow disturbance, etc., so that a lot of efforts will be needed to come up with a stable and reliable system.

Acknowledgement

The authors thank Prof. Henry Baltes (emeritus) for his interest in their work. Funding was provided by the Swiss Federal Office for Science and Education (BBW) within the EU project Biofinger, IST-2001-34544.

References

[1] R. Berger, E. Delamarche, H.P. Lang, C. Gerber, J.K. Gimzewski, E. Meyer, H.J. Güntherodt, Surface stress in the self-assembly of alkanethiols on gold, Science 276 (1997) 2021–2024.
[2] J.K. Gimzewski, C. Gerber, E. Meyer, R.R. Schlittler, Observation of a chemical-reaction using a micromechanical sensor, Chem. Phys. Lett. 217 (1994) 589–594.
[3] J.K. Gimzewski, S. Modesti, R.R. Schlittler, Cooperative self-assembly of au atoms and C(60) on Au(110) surfaces, Phys. Rev. Lett. 72 (1994) 1036–1039.
[4] F.M. Battiston, J.P. Ramseyer, H.P. Lang, M.K. Baller, C. Gerber, J.K. Gimzewski, E. Meyer, H.J. Güntherodt, A chemical sensor based on a microfabricated cantilever array with simultaneous resonance–frequency and bending readout, Sens. Actuators B: Chem. 77 (2001) 122–131.

[5] A. Boisen, J. Thaysen, H. Jensenius, O. Hansen, Environmental sensors based on micromachined cantilevers with integrated read-out, Ultramicroscopy 82 (2000) 11–16.
[6] C.L. Britton Jr., R.L. Jones, P.I. Oden, Z. Hu, R.J. Warmack, S.F. Smith, W.L. Bryan, J.M. Rochelle, Multiple-input microcantilever sensors, Ultramicroscopy 82 (2000) 17–21.
[7] C.L. Britton Jr., R.J. Warmack, S.F. Smith, P.I. Oden, G.M. Brown, W.L. Bryan, L.G. Clonts, M.G. Duncan, M.S. Emery, M.N. Ericson, Z. Hu, R.L. Jones, M.R. Moore, J.A. Moore, J.M. Rochelle, T.D. Threatt, T. Thundat, G.W. Turner, A.L. Wintenberg, MEMS sensors and wireless telemetry for distributed systems, Proc. SPIE 3328 (1998) 112–123.
[8] H. Jensenius, J. Thaysen, A.A. Rasmussen, L.H. Veje, O. Hansen, A. Boisen, A microcantilever-based alcohol vapor sensor-application and response model, Appl. Phys. Lett. 76 (2000) 2615–2617.
[9] B.H. Kim, M. Maute, F.E. Prins, D.P. Kern, M. Croitoru, S. Raible, U. Weimar, W. Göpel, Parallel frequency readout of an array of mass-sensitive transducers for sensor applications, Microelectron. Eng. 53 (2000) 229–232.
[10] B.H. Kim, F.E. Prins, D.P. Kern, S. Raible, U. Weimar, Multicomponent analysis and prediction with a cantilever array based gas sensor, Sens. Actuators B: Chem. 78 (2001) 12–18.
[11] H.P. Lang, M.K. Baller, F.M. Battiston, J. Fritz, R. Berger, J.P. Ramseyer, P. Fornaro, E. Meyer, H.J. Guntherodt, J. Brugger, U. Drechsler, H. Rothuizen, M. Despont, P. Vettiger, C. Gerber, J.K. Gimzewski, The nanomechanical nose technical digest, in: IEEE International MEMS'99 Conference, 12th IEEE International Conference on Micro Electro mechanical Systems, Zurich Res. Lab. IBM Res. Div. Ruschlikon Switzerland, Orlando, FL, USA, IEEE Robotics & Autom. Soc, 1999, pp. 9–13.
[12] H.P. Lang, M. Hegner, C. Gerber, Nanomechanics—the link to biology and chemistry, Chimia 56 (2002) 515–519.
[13] D. Lange, C. Hagleitner, A. Hierlemann, O. Brand, H. Baltes, Complementary metal oxide semiconductor cantilever arrays on a single chip: mass-sensitive detection of volatile organic compounds, Anal. Chem. 74 (2002) 3084–3095.
[14] M. Maute, S. Raible, F.E. Prins, D.P. Kern, H. Ulmer, U. Weimar, W. Göpel, Detection of volatile organic compounds (VOCs) with polymer-coated cantilevers, Sens. Actuators B: Chem. 58 (1999) 505–511.
[15] J. Thaysen, R. Marie, A. Boisen, Cantilever-based bio-chemical sensor integrated in a microliquid handling system, in: Technical Digest, MEMS'2001, 14th IEEE International Conference on Micro Electro Mechanical Systems, Mikroelektronik Centret Tech. Univ. Denmark Lyngby Denmark, Interlaken, Switzerland, 2001, pp. 401–404.
[16] C. Vancura, M. Ruegg, Y. Li, C. Hagleitner, A. Hierlemann, Magnetically actuated complementary metal oxide semiconductor resonant cantilever gas sensor systems, Anal. Chem. 77 (2005) 2690–2699.
[17] M. Alvarez, J. Tamayo, Optical sequential readout of microcantilever arrays for biological detection, Sens. Actuators B: Chem. 106 (2005) 687–690.
[18] M. Calleja, J. Tamayo, A. Johansson, P. Rasmussen, L.M. Lechuga, A. Boisen, Polymeric cantilever arrays for biosensing applications, Sens. Lett. 1 (2003) 20–24.
[19] L.M. Lechuga, J. Tamayo, M. Alvarez, L.G. Carrascosa, A. Yufera, R. Doldan, E. Peralias, A. Rueda, J.A. Plaza, K. Zinoviev, C. Dominguez, A. Zaballos, M. Moreno, C. Martinez, D. Wenn, N. Harris, C. Bringer, V. Bardinal, T. Camps, C. Vergnenegre, C. Fontaine, V. Diaz, A. Bernad, A highly sensitive microsystem based on nanomechanical biosensors for genomics applications, Sens. Actuators B: Chem. 118 (2006) 2–10.
[20] J. Tamayo, Study of the noise of micromechanical oscillators under quality factor enhancement via driving force control, J. Appl. Phys. 97 (2005).
[21] J. Tamayo, D. Ramos, J. Mertens, M. Calleja, Effect of the adsorbate stiffness on the resonance response of microcantilever sensors, Appl. Phys. Lett. 89 (2006).
[22] C. Vancura, Y. Li, J. Lichtenberg, K.U. Kirstein, A. Hierlemann, F. Josse, Liquid-phase chemical and biochemical detection using fully integrated magnetically actuated complementary metal oxide semiconductor resonant cantilever sensor systems, Anal. Chem. 79 (2007) 1646–1654.
[23] J. Fritz, M.K. Baller, H.P. Lang, H. Rothuizen, P. Vettiger, E. Meyer, H.J. Güntherodt, C. Gerber, J.K. Gimzewski, Translating biomolecular recognition into nanomechanics, Science 288 (2000) 316–318.
[24] K.M. Hansen, T. Thundat, Microcantilever biosensors, Methods 37 (2005) 57–64.
[25] H.F. Ji, X.D. Yan, J. Zhang, T. Thundat, Molecular recognition of biowarfare agents using micromechanical sensors, Expert Rev. Mol. Diagn. 4 (2004) 859–866.
[26] F. Tian, K.M. Hansen, T.L. Ferrell, T. Thundat, Dynamic microcantilever sensors for discerning biomolecular interactions, Anal. Chem. 77 (2005) 1601–1606.
[27] X.D. Yan, H.F. Ji, T. Thundat, Microcantilever (MCL) biosensing, Curr. Anal. Chem. 2 (2006) 297–307.
[28] C. Vancura, J. Lichtenberg, A. Hierlemann, F. Josse, Characterization of magnetically actuated resonant cantilevers in viscous fluids, Appl. Phys. Lett. 87 (2005).
[29] E. Forsen, G. Abadal, S. Ghatnekar-Nilsson, J. Teva, J. Verd, R. Sandberg, W. Svendsen, F. Perez-Murano, J. Esteve, E. Figueras, F. Campabadal, L. Montelius, N. Barniol, A. Boisen, Ultrasensitive mass sensor fully integrated with complementary metal-oxide-semiconductor circuitry, Appl. Phys. Lett. 87 (2005) 043507.
[30] S. Ghatnekar-Nilsson, E. Forsen, G. Abadal, J. Verd, F. Campabadal, F. Perez-Murano, J. Esteve, N. Barniol, A. Boisen, L. Montelius, Resonators with integrated CMOS circuitry for mass sensing applications, fabricated by electron beam lithography, Nanotechnology 16 (2005) 98–102.
[31] G.Y. Chen, T. Thundat, E.A. Wachter, R.J. Warmack, Adsorption-induced surface stress and its effects on resonance frequency of microcantilevers, J. Appl. Phys. 77 (1995) 3618–3622.
[32] M. Sepaniak, P. Datskos, N. Lavrik, C. Tipple, Microcantilever transducers: a new approach to sensor technology, Anal. Chem. 74 (2002) 568A–575A.
[33] T. Volden, CMOS-integrated cantilevers for biosensing and probe microscopy, Dissertation 15984, ETH Zurich, 2005. Available online via: http://e-collection.ethbib.ethz.ch/cgi-bin/show.pl?type=diss&nr=15984.
[34] C. Menolfi, Q. Huang, A low noise CMOS chopper instrumentation amplifier for thermoelectric infrared detectors, IEEE J. Solid State. Circ. 32 (1997) 968–976.
[35] J.J.F. Rijns, CMOS low-distortion high-frequency variable-gain amplifier, IEEE J. Solid State Circ. 31 (1996) 1029–1034.
[36] P.E. Allen, D.R. Holberg, CMOS Analog Circuit Design, Oxford University Press, Oxford, UK, 2002, pp. 126–134.
[37] E. Säckinger, W. Guggenbühl, A high-swing, high-impedance MOS cascade circuit, IEEE J. Solid State Circ. 25 (1990) 289–298.
[38] C. Menolfi, Low noise CMOS chopper instrumentation amplifier for thermoelectric microsensors. Dissertation ETH Zurich No. 13583, 2000. Accessible via Internet: http://e-collection.ethbib.ethz.ch/cgi-bin/show.pl?type=diss&nr=13583.
[39] Philips Semiconductors, Eindhoven, the Netherlands, see: http://www.semiconductors.philips.com/markets/mms/protocols/i2c/facts/.
[40] T. Müller, M. Brandl, O. Brand, H. Baltes, An industrial CMOS process family adapted for the fabrication of smart silicon sensors, Sens. Actuators A: Phys. 84 (2000) 126–133.
[41] R. Buchhold, A. Nakladal, G. Gerlach, P. Neumann, Design studies on piezoresistive humidity sensors, Sens. Actuators B: Chem. 53 (1998) 1–7.
[42] R. Buchhold, A. Nakladal, G. Gerlach, K. Sahre, K.J. Eichhorn, M. Muller, Reduction of mechanical stress in micromachined components caused by humidity-induced volume expansion of polymer layers, Microsyst. Technol. 5 (1998) 3–12.
[43] R. Buchhold, A. Nakladal, U. Buttner, G. Gerlach, The metrological behaviour of bimorphic piezoresistive humidity sensors, Meas. Sci. Technol. 9 (1998) 354–359.
[44] T. Boltshauser, CMOS humidity sensors, PhD Thesis, ETH Zurich No. 10320, Zurich, Switzerland, 1993.
[45] H. Jensenius, Microcantilever-based studies of bio/chemical systems, PhD Thesis, Mikroelektronik Centret, Technical University of Denmark, Copenhagen, Denmark, 2002.
[46] K. Bodenhöfer, A. Hierlemann, R. Schlunk, W. Göpel, New method of vaporizing volatile organics for gas tests, Sens. Actuators B 45 (1997) 259–264.
[47] J.A. Riddick, W.B. Bunger, T.K. Sakano, Organic Solvents, Wiley Interscience, New York, NY, USA, 1986.

[48] A.M. Kummer, T.P. Burg, A. Hierlemann, Transient signal analysis using complementary metal oxide semiconductor capacitive chemical microsensors, Anal. Chem. 78 (2006) 279–290.
[49] P. Kurzawski, C. Hagleitner, A. Hierlemann, Detection and discrimination capabilities of a multi-transducer single-chip gas sensor system, Anal. Chem. 78 (2006) 6910–6920.
[50] A.M. Kummer, A. Hierlemann, H. Baltes, Tuning sensitivity and selectivity of complementary metal oxide semiconductor-based capacitive chemical microsensors, Anal. Chem. 76 (2004) 2470–2477.

Biographies

Martin Zimmermann received the diploma degree in electrical engineering from the University of Applied Sciences, Rapperswil, Switzerland, 1996. From 1996 to 2005, he was involved in the development of mixed-signal circuitry for CMOS sensor systems at the Physical Electronics Laboratory of ETH Zurich, Switzerland. In 2006, he joined the Camille Bauer AG, Wohlen, Switzerland, where his current activities are focused on capacitive angular displacement sensors.

Tormod Volden received the Ingénieur Diplômé degree in engineering physics from the Institut National des Sciences Appliquées, Toulouse, France in 1995 and then worked as a staff engineer at the Norwegian Radium Hospital, Oslo, Norway. From 2000 on he was a research assistant at the Physical Electronics Laboratory of ETH Zurich and received the PhD degree for his thesis entitled "CMOS-integrated sensors for atomic-force microscopy and biochemical detection" in 2005. Since then he is working for the company Osmotex in Alpnach, Switzerland, developing microfluidic actuators.

Kay-Uwe Kirstein received the diploma in electrical engineering from the University of Technology Hamburg-Harburg (TUHH), Germany, in 1997 and the Ph.D. degree from the University of Duisburg, Germany, in 2001. He was a Research Associate with the Fraunhofer Institut of Microelectronic Circuits and Systems in Dresden and worked in the analog circuit design group at Micronas GmbH, Freiburg, Germany. Afterwards he has been team leader of the circuit design group at the Physical Electronics Laboratory, ETH Zurich and is now with Miromico AG, Zurich, Switzerland.

Sadik Hafizovic received the diploma degree in microsystem technology from IMTEK, University of Freiburg, Germany, in 2002 and the Ph.D. degree in electrical engineering from ETH Zurich, Switzerland, in 2007. He worked on his diploma thesis in the Tabata Laboratories at the Ritsumeikan University, Japan in 2002. He is currently a Postdoc at the Physical Electronics Laboratory, ETH Zurich, Switzerland. The focus of his research activities is on atomic-force microscopy and CMOS-based microelectrode arrays for neuronal interfaces.

Jan Lichtenberg received his M.S. degree in electrical engineering and microtechnology from the University Bremen, Germany in 1998 and a Ph.D. in 2002 from the Institute of Microtechnology at the University of Neuchâtel in Switzerland. Subsequently, he joined the Laboratory for Physical Electronics (PEL) at the Swiss Federal Institute of Technology (ETH) in Zurich, Switzerland as a team leader. His research interests are microfluidics for bio-chemical analysis and cell handling, CMOS-based micromechanical sensor for clinical diagnostics, as well as packaging and integration issues. Jan Lichtenberg is also founder and CEO of AMMT Inc., a leading supplier of wet-etching equipment for microtechnology, and CTO of UWATEC AG, Switzerland.

Oliver Brand received his diploma degree in Physics from the Technical University of Karlsruhe, Germany in 1990, and his Ph.D. degree (Doctor of Natural Sciences) from ETH Zurich, Switzerland in 1994. From 1995 to 1997, he worked as a postdoctoral fellow at the Georgia Institute of Technology in Atlanta, GA, USA. From 1997 to 2002, he was a lecturer at ETH Zurich, Switzerland and a research group leader in the Physical Electronics Laboratory (PEL). In January 2003 he joined the Electrical & Computer Engineering faculty at the Georgia Institute of Technology in Atlanta, GA, USA, as an associate professor. His research interests include CMOS-based microsystems and microsensors, MEMS fabrication technologies, and microsystem packaging.

Andreas Hierlemann received his diploma in chemistry in 1992 and the Ph.D. degree in physical chemistry in 1996 from the University of Tübingen, Germany. After working as a Postdoc at Texas A&M University, College Station, TX (1997), and Sandia National Laboratories, Albuquerque, NM (1998), he is currently associate professor at the Physical Electronics Laboratory at ETH Zurich in Switzerland. The focus of his research activities is on CMOS-based microsensors and interfacing CMOS electronics with electrogenic cells.